Supporting Information for 'Phytoplankton blooms at increasing levels of atmospheric carbon dioxide: experimental evidence for negative effects on prymnesiophytes and positive on small picoeukaryotes'

S-3 Methods

S-3.1 pH dye preparation, measurements and corrections

Determination of seawater pH followed in principle the spectrophotometrical approach of Clayton and Byrne (1993) described in Dickson, A. G. and Sabine, C. L. and Christian, J.R. (Eds.) (2007) making use of the dye m-cresol purple (Acros Organics, CAS 62625-31-4, Lot A026431) at 25°C in a 10 cm thermostated cuvette on a Cary 100 (Varian). Concerning the dye, 300 ml of an about 2 mM solution was prepared in Milli-Q, the ionic strength brought to 0.66 with NaCl (matching that of seawater with a salinity of $\sim$32) and the $\mathrm{pH_T}$ (pH on the total scale) adjusted to about 7.6 (at 25°C). After that the solution was sterile filtered (0.2 μm) into a gas and light impermeable sampling bag (Supelco), filled without air.

For measurements, 5 ml of sample water was pumped from the bottom of a 100 ml bottle, brought to 25°C in a thermostated water bath, into a 25 ml syringe pump (Tecan, Cavro XLP 6000), followed by about 50 μl of m-cresol purple dye solution, and then mixed within the syringe with an additional 15 ml of sample water. This mixture was then injected into the 10 cm flow-through cuvette (with a capacity of about 8 ml), which had been previously filled

carefully whiteout air bubbles with filtered (0.2 μm) fjord water, or already contained sample water. Samples were measured from low to high fCO_2, and potential carry-over from a previous sample was usually below detection limit. Each seawater sample was measured in triplicates and precision of replicate measurements was typically 0.001 or better for the higher and 0.002 or better for the lower pH treatments (with the threshold at an in situ pH of about 7.700). Measured absorption spectra (780 to 380 nm at 1nm resolution and a scan rate of 600 nm per minute) were corrected for tiny air bubble entrainment by comparison to an absorption mean between 735 and 725 nm, wavelengths at which the dye is non-absorbent, of a baseline in Milli-Q. The resulting absorption ratio at 578 and 434 nm was then used to calculate pH_T using the acid dissociation constant and extinction coefficient ratios of m-cresol purple reported in Dickson, A. G. and Sabine, C. L. and Christian, J.R. (Eds.) (2007). Furthermore, absorbance at 578 nm, the isosbestic point, was used to correct the calculated pH by accounting for inevitable changes due to dye addition (about -0.005 pH units at the highest and +0.014 at the lowest pH), similar to the method described in Clayton and Byrne (1993). For that purpose five seawater batches of different pH, one liter each, covering the entire measurement range, were prepared, and in each pH was determined as described above, but with increasing amounts of dye (six levels). At each pH level a linear correlation between the change in pH in relation to the absorbance at the isosbestic point (a measure for the amount of dye added) was constructed. The combination of all six correlations at each pH level then led to an uniform linear relation describing the change in measured pH in response to a certain amount of dye added at a certain pH.

To assess the accuracy of pH measurements, and to account for potential impurities in the m-cresol purple sodium salt, pH_T was measured and corrected as described above on five replicates of CRM batch 108 (freshly opened). However, no further corrections were applied

as measured $\mathrm{pH_T}$ (7.8791 ± 0.0002) was off less then 0.001 units the theoretical one of 7.8786, calculated from known DIC (2022.7 $\mu\mathrm{mol\,kg^{-1}}$), total alkalinity, TA (2218.0 $\mu\mathrm{mol\,kg^{-1}}$), salinity (33.224), phosphate (0.41 $\mu\mathrm{mol\,kg^{-1}}$) and silicate (2.9 $\mu\mathrm{mol\,kg^{-1}}$) concentrations using the dissociation constants for carbonic acid from Mehrbach et al. (1973) as refitted by Lueker et al. (2000).

S-3.2 pH sample filtration

Prior to analysis samples for pH were transferred from the 500 ml glass stoppered bottles (Schott Duran) with a membrane pump to 100 ml glass stoppered bottles (Schott Duran) at a flow rate of about 50 ml per minute, passing a sterile 0.2 $\mu\mathrm{m}$ filter (Sarstedt Filtropur, PES membrane). For that the sample water was pumped from the bottom of the 500 ml bottles, filling the 100 ml bottles through a serological needle from bottom to top with about 100 ml of additional overflow. Since about 300 ml of sample water always remained in the larger bottles, tubing was Tygon and the smaller bottles were filled from bottom to top with considerable overflow, potential $\mathrm{CO_2}$ gas exchange with the atmosphere, impacting seawater pH, was minimized. Filtration removed all particulate organic matter which, at relatively high concentrations, can influence the precision of spectrophotometric measurements. Furthermore, the close to sterile seawater samples are relatively stable as potential biological activity by phytoplankton or bacteria, otherwise impacting pH, is minimized. The 100 ml bottles were closed without headspace and, if not measured within the next couple of hours, stored at $4^{\circ}\mathrm{C}$ in the dark.

S-3.3 Carbonate chemistry calculations

In a first step measured $\mathrm{pH_T}$ (at 25°C) and DIC was used to calculate practical alkalinity (PA). The second step involved calculating $\mathrm{pH_T}$ and all the other carbonate chemistry components such as the fugacity of carbon dioxide, $\mathrm{fCO_2}$, at in-situ temperature and salinity conditions from measured DIC and calculated PA, using the dissociation constants for carbonic acid from Mehrbach et al. (1973) as refitted by Lueker et al. (2000). Since there were no DIC and spectrophotometric pH measurements on the first three (t-3 to t-1) and last six days (28 to 34), carbonate chemistry speciation had to be estimated using CTD-derived mean water column pH measurements, brought to the total scale with CTD to spectrophotometric pH relations for day 0 and 27 (compare section 3.5), and salinity based estimates of PA. For that purpose, mean water column salinity changes were considered a proxy for changes in PA, taking a mean initial PA of 2180 $\mu\mathrm{mol\,kg^{-1}}$ and a mean initial salinity of 31.95. The assumption that the sole drivers of TA changes are freshwater input by rain and evaporation obviously ignores the impact of phosphate and nitrate assimilation and calcium carbonate production on TA. Nevertheless, here estimates of carbonate chemistry speciation will hardly be affected as 1) changes in alkalinity due to nutrient assimilation (about +5 $\mu\mathrm{mol\,kg^{-1}}$) and calcification (maximum of -2 $\mu\mathrm{mol\,kg^{-1}}$), which furthermore work in opposite directions, were smaller than those by freshwater input (about -9 $\mu\mathrm{mol\,kg^{-1}}$) and 2) the estimates are based on measured pH, rendering the carbonate system practically insensitive to even relatively large PA uncertainties (depending on actual $\mathrm{CO_2}$ level, 10 $\mu\mathrm{mol\,kg^{-1}}$ correspond to only a few $\mu\mathrm{atm}$).

S-4 Results

S-4.1 Changes in light, salinity and temperature

Average incident photosynthetic active radiation (PAR) measured in air was similar during all phases, although slightly higher during the first two weeks (Fig. S-3). Light profiles taken within and outside the mesocosms were generally very similar, with marginally higher attenuation in the upper 10 m of the mesocosms, possibly due to shading by the floating structures, and potentially higher particulate biomass (Fig. S-3b). Nevertheless, no significant differences were observed between mesocosms and through time (data not shown), while attenuation coefficients were similar in comparison to a previous KOSMOS study, with typical k_d values between 0.3 and 0.4 (Schulz et al., 2013). Using an average incident PAR intensity of 450 $\mu\mathrm{mol\,m^{-2}s^{-1}}$ during daylight, depth-averaged (0.3-23 m) light conditions were about 56 $\mu\mathrm{mol\,m^{-2}s^{-1}}$. This is probably at least three times lower then in two previous mesocosm experiments at the same location in bags of only 5 (Engel et al., 2005) and 10 meters depth Schulz et al. (2008).

Depth-averaged salinity in the fjord ranged from 30.20 to 31.54, thus being more variable than in the mesocosms (Fig. S-2a). Ignoring the initial salt addition for volume determinations, depth-integrated variability within the mesocosms was about 0.15 salinity units, and while being relatively stable throughout the first 2 weeks, constantly decreased towards the end of the experiment. This decrease was most likely due to rain water input as most pronounced in the upper 5-10 m of the mesocosms (Fig. S-2b). Overall dilution by rainwater was on the order of 5‰.

Average water column temperatures steadily increased within the mesocosms and the fjord, from initially about 7 to 10°C half way through the experiment (Fig S-2c). Although surface

waters continued to warm, upwelling of colder deeper waters in the fjord to up to 15 m depth, also mirrored in salinity changes (Fig S-2a), kept average temperatures relatively constant until the end of the experiment. Average temperatures did not significantly exceed 10°C, and reached up to 13°C in the upper meter by the end of the experiment Fig S-2c).

References

Clayton, T. D. and Byrne, R. H. (1993). Spectrophotometric seawater pH measurements: total hydrogen ion concentration scale calibrations of *m*-cresol purple and at-sea results. *Deep-Sea Res.* 40, 2115–2129

Dickson, A. G. and Sabine, C. L. and Christian, J.R. (Eds.) (2007). Guide to Best Practices for Ocean CO_2 Measurements. *PICES Special Publication 3*

Engel, A., Zondervan, I., Aerts, K., Beaufort, L., Benthien, A., Chou, L., et al. (2005). Testing the direct effect of CO_2 concentration on a bloom of the coccolithophorid *Emiliania huxleyi* in mesocosm experiments. *Limnol. Oceanogr.* 50, 493–507

Lueker, T. J., Dickson, A. G., and Keeling, C. D. (2000). Ocean pCO_2 calculated from dissolved inorganic carbon, alkalinity, and equations for K_1 and K_2: validation based on laboratory measurements of CO_2 in gas and seawater at equilibrium . *Mar. Chem.* 70, 105–119

Mehrbach, C., Culberson, C. H., Hawley, J. E., and Pytkowicz, R. M. (1973). Measurements of the apparent dissociation constants of carbonic acid in seawater at atmospheric pressure. *Limnol. Oceanogr.* 18, 897–907

Schulz, K. G., Bellerby, R. G. J., Brussaard, C. P. D., Büdenebnder, J., Czerny, J., Engel, A., et al. (2013). Temporal biomass dynamics of an Arctic plankton bloom in response to increasing levels of atmospheric carbon dioxide. *Biogeosci.* 10, 161–180

Schulz, K. G., Riebesell, U., Bellerby, R. G. J., Biswas, H., Meyeröfer, M., Müller, M. N., et al. (2008). Build-up and decline of organic matter during PeECE III. *Biogeosci.* 5, 707–718

Table S-1: R^2, F and p values for statistically significant correlations ($p < 0.05$) between the mean of a measurement parameter and fCO_2 during a certain phase of the experiment. For details see section 3.8. Positive correlations are shown in bold, negative in italic (in total 60 out of 160). Superscripts [a], [b], [c], [d], and [f] refer to data shown in Figs. 3, S-5, 4, 5, S-6, respectively

	Phase I			Phase II			Phase III			Phase IV		
	adj. R^2	F	p	adj. R^2	F	p	adj. R^2	F	p	adj. R^2	F	p
[a,d]Chl$a$	**0.7598**	**23.14**	**0.003**	*0.6734*	*15.43*	*0.008*						
[b]POC	**0.7002**	**15.02**	**0.012**									
[b]PON	**0.5120**	**8.34**	**0.028**									
[b]POP	**0.7583**	**22.96**	**0.003**	**0.7561**	**22.70**	**0.003**						
[b]BSi												
[b]DOC										*0.5041*	*8.12*	*0.029*
[b]DON												
[b]DOP	*0.5268*	*8.79*	*0.025*				**0.5260**	**8.77**	**0.025**			
[a]Nitrate	*0.4199*	*6.07*	*0.049*									
[a]Ammonia	*0.7633*	*23.57*	*0.003*	*0.8037*	*29.66*	*0.002*						
[a]Phosphate				*0.5579*	*9.835*	*0.020*						
[a]Silicate												
[a]$\Delta[O_2]$							*0.6027*	*11.62*	*0.014*	*0.7360*	*20.51*	*0.004*

Tab. continued

	Phase I			Phase II			Phase III			Phase IV		
	adj. R^2	F	p	adj. R^2	F	p	adj. R^2	F	p	adj. R^2	F	p
[c]Chla_{Hapto}				*0.8215*	*33.23*	*0.001*	*0.4451*	*6.62*	*0.042*	*0.8032*	*29.56*	*0.002*
[c]Chla_{Chryso}				*0.5287*	*8.85*	*0.025*						
[c]Chla_{Dino}												
[c]Chla_{Diatom}							*0.6998*	*17.31*	*0.006*			
[c]Chla_{Chloro}	**0.9055**	**68.06**	**<0.001**	**0.8454**	**39.27**	**<0.001**	**0.6656**	**14.93**	**0.008**	**0.5238**	**8.70**	**0.026**
[c]Chla_{Crypto}				*0.7646*	*23.74*	*0.003*						
[c]Chla_{Cyano}	**0.4613**	**6.99**	**0.038**	**0.7739**	**24.97**	**0.003**	**0.9391**	**108.9**	**<0.001**	**0.7984**	**28.73**	**0.002**
[d]Syn$_{\text{FCM}}$	**0.5633**	**10.03**	**0.019**	**0.4820**	**7.52**	**0.034**	**0.9212**	**82.81**	**<0.001**	**0.7292**	**19.85**	**0.004**
[d]Pico$_{\text{FCM}}$	**0.8590**	**43.63**	**<0.001**	**0.9560**	**153.15**	**<0.001**	**0.8948**	**60.56**	**<0.001**	**0.6879**	**16.43**	**0.007**
[d]Ehux$_{\text{FCM}}$				*0.6805*	*15.92*	*0.007*	*0.4631*	*7.04*	*0.038*	*0.4412*	*6.53*	*0.043*
[d]Nano small$_{\text{FCM}}$							*0.5137*	*8.39*	*0.030*			
[d]Nano big$_{\text{FCM}}$				*0.5936*	*11.23*	*0.015*	*0.8702*	*47.93*	*< 0.001*			
[d]Crypto$_{\text{FCM}}$				*0.6614*	*14.67*	*0.009*						
[e]Hapto$_{\text{Micro}}$				*0.6952*	*16.96*	*0.006*	*0.5874*	*10.96*	*0.016*	n.a.	n.a.	n.a.
[e]Dino NT$_{\text{Micro}}$				*0.6366*	*13.26*	*0.011*				n.a.	n.a.	n.a.
[e]Dino T$_{\text{Micro}}$										n.a.	n.a.	n.a.
[f]Diatom$_{\text{Micro}}$							*0.7707*	*24.52*	*0.003*	n.a.	n.a.	n.a.
[e]Chloro$_{\text{Micro}}$				**0.6246**	**12.65**	**0.012**				n.a.	n.a.	n.a.
[e]Crypto$_{\text{Micro}}$										n.a.	n.a.	n.a.
[e]Dino HT$_{\text{Micro}}$				**0.5171**	**8.50**	**0.027**				n.a.	n.a.	n.a.
[e]Tot. auto$_{\text{Micro}}$							*0.8422*	*36.36*	*< 0.001*	n.a.	n.a.	n.a.

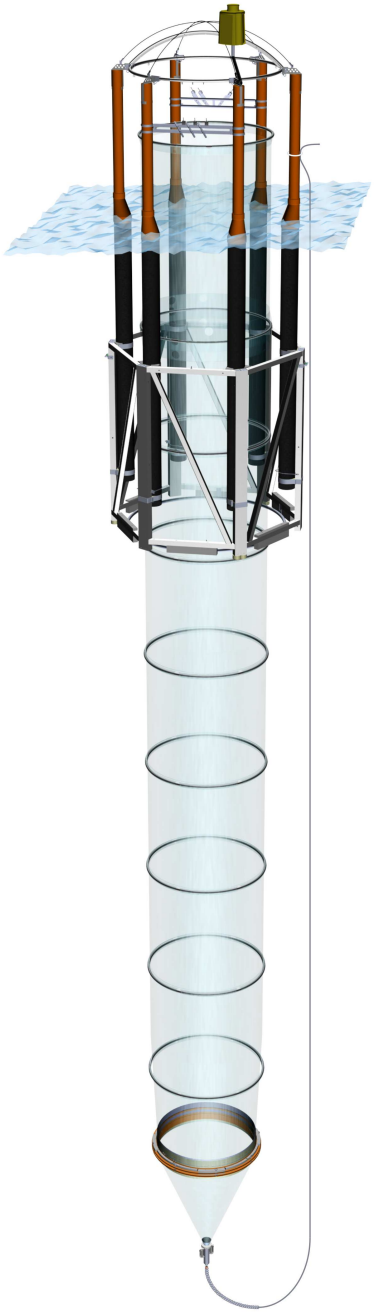

Figure S-1: Schematic drawing of a KOSMOS mesocosm deployed in Raunefjorden, Norway. The orange flanges at depth connect the funnel-shaped sediment trap to the rest of the bag.

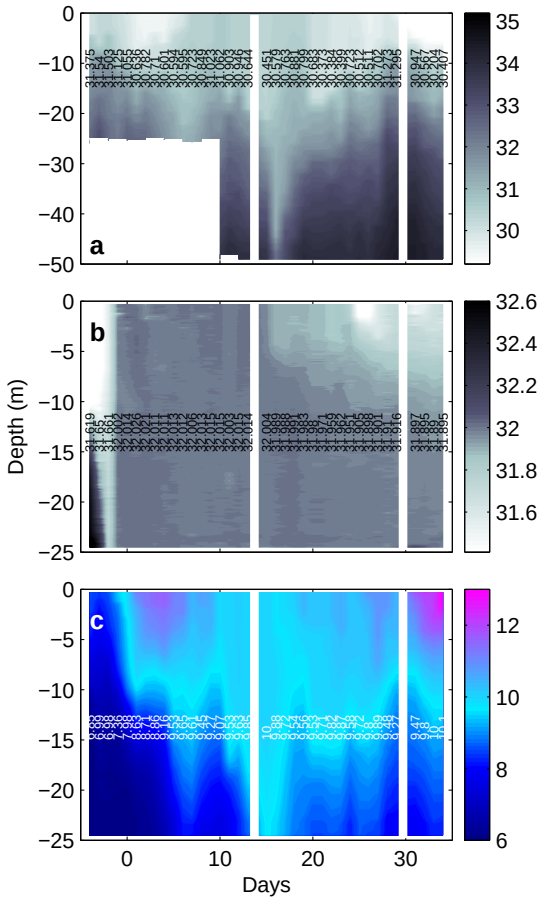

Figure S-2: Vertical distribution and dynamics of salinity measured in the fjord **(a)** and mesocosm M9 **(b)** together with those of temperature **(c)**, given in degrees Celsius. Note that with the exception of mesocosm M2 which had a hole right from the beginning, allowing fjord and mesocosm water to exchange, temperature and salinity dynamics in all other mesocosms were practically identical. Numbers represent depth-averaged (0.3-23 m) values.

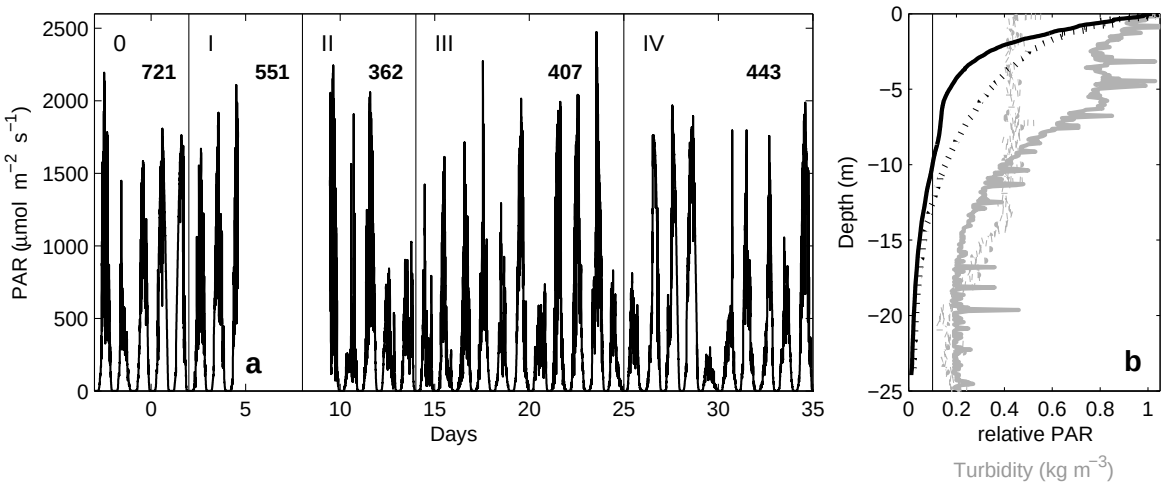

Figure S-3: (a) Changes in photosynthetic active radiation (PAR) in air, and **(b)** a typical vertical light (black) and turbidity (grey) profile in a mesocosm (solid lines) and the fjord (dotted lines). Numbers in **(a)** denote average daily PAR levels during a certain phase, indicated by vertical lines and Roman numbers. In **(b)** the vertical line marks the 10% level of incident light. For details on measurements see section 3.5.

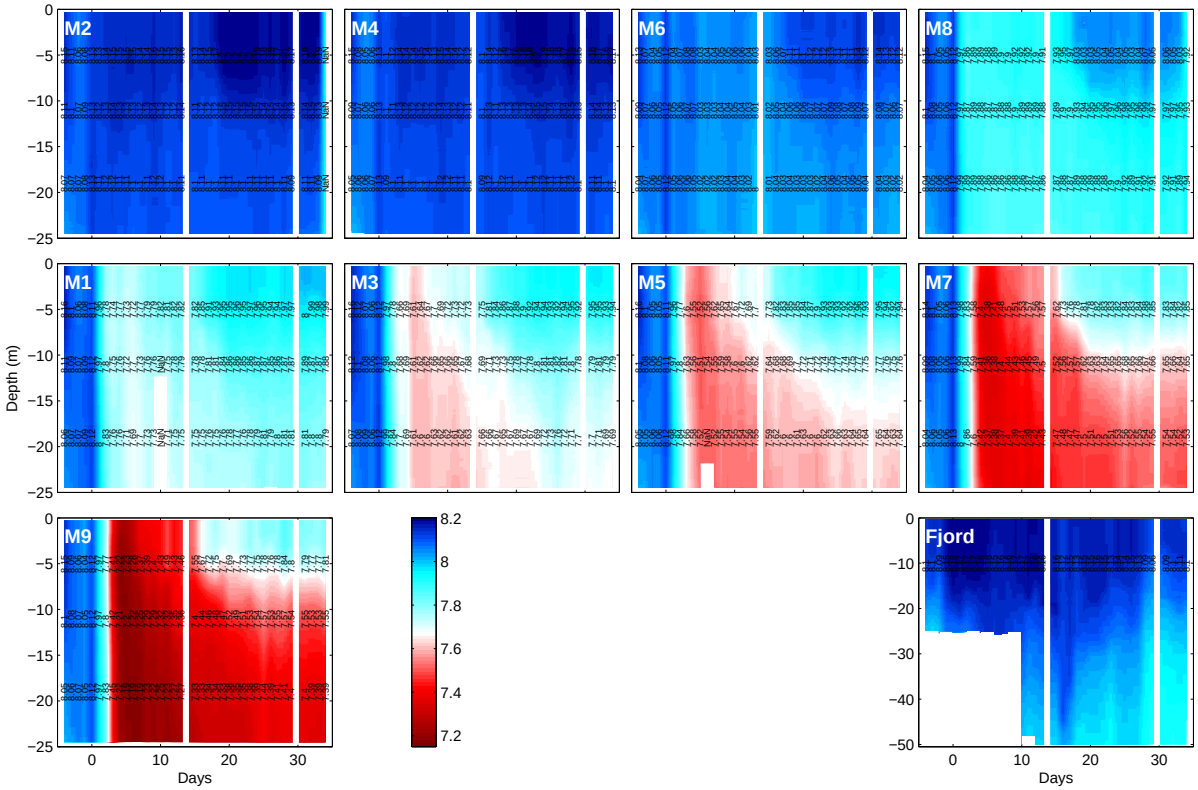

Figure S-4: Temporal development of pH (corrected to the total scale) in the mesocosms and the fjord as measured by a hand-operated CTD. Numbers at -5, -11 and -19 m depth denote daily averages representative for 0.3-5 m, 0.3-23 m and 15-23 m, respectively. For details on pH corrections applied see section 3.5.

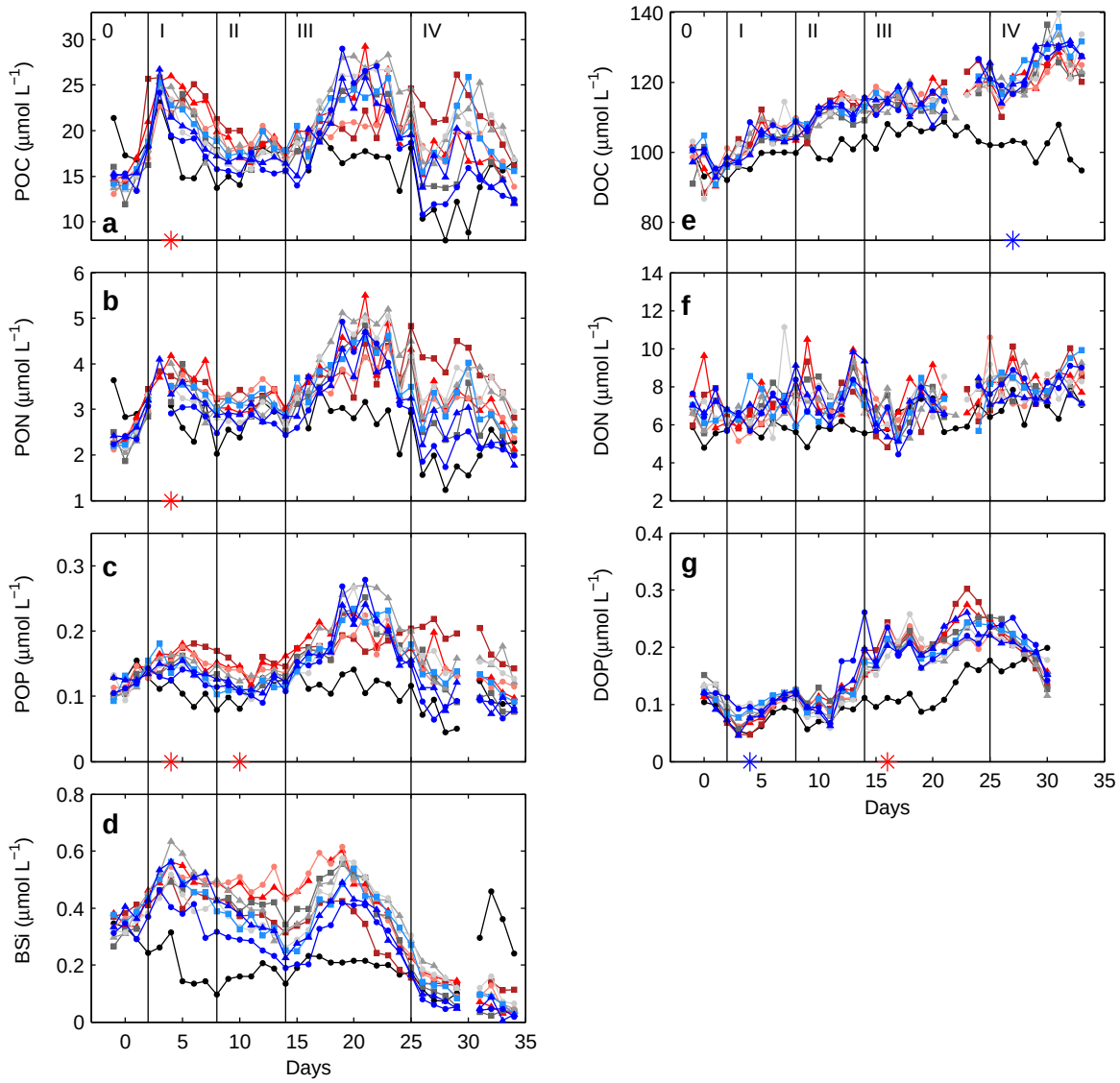

Figure S-5: Temporal dynamics of depth-integrated (0-23 m) POC **(a)**, PON **(b)**, POP **(c)**, BSi **(d)**, DOC **(e)**, DON **(f)** and DOP **(g)** inside the fjord and the mesocosms. Note that concentrations for DOP have been smoothed by applying a three day running mean. Style and color coding follow that of Fig. 2.

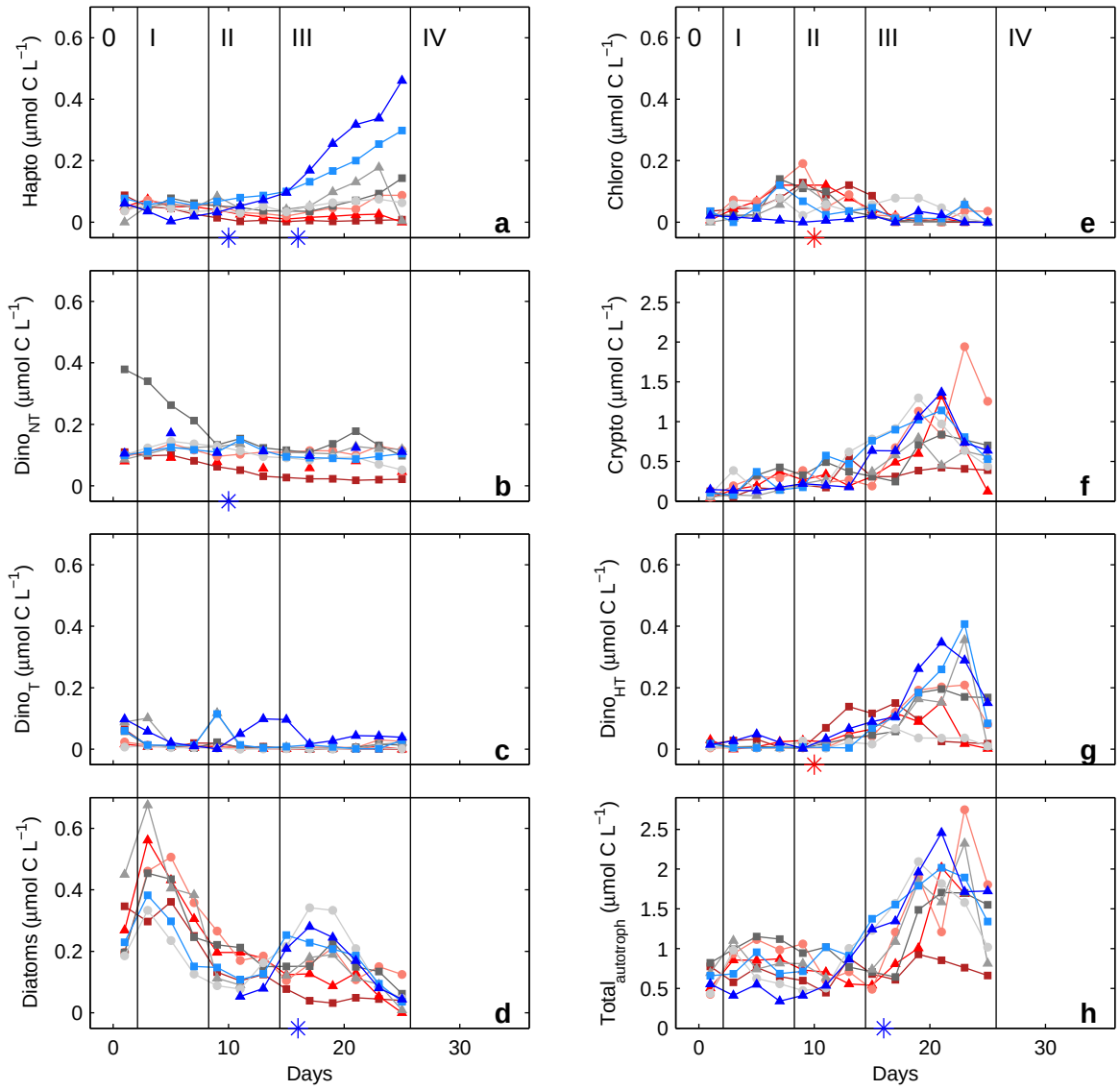

Figure S-6: Temporal dynamics of depth-integrated (0-23 m) organic carbon biomass of haptophytes **(a)**, non-toxic dinoflagellates **(b)**, toxic dinoflagellates **(c)**, diatoms **(d)**, chlorophytes **(e)**, cryptophytes **(f)** and heterotrophic dinoflagellates **(g)** in side the fjord and the mesocosms, as determined by microscopy (see section 3.6 for details). The sum of the total autotrophic biomass is also shown **(h)**. Style and color coding follow that of Fig. 2.